

Magnetism of chromia

Siqi Shi,* A. L. Wysocki, and K. D. Belashchenko

*Department of Physics and Astronomy and Nebraska Center for Materials and Nanoscience,
University of Nebraska–Lincoln, Lincoln, Nebraska 68588, USA*

(Dated: October 19, 2018)

The electronic structure and magnetism of chromia (corundum-type Cr_2O_3) are studied using full-potential first-principles calculations. The electronic correlations are included within the LSDA+U method. The energies of different magnetic configurations are very well fitted by the Heisenberg Hamiltonian with strong exchange interaction with two nearest neighbors and additional weak interaction up to the fifth neighbor shell. These energies are insensitive to the position of the oxygen states, indicating that magnetism in Cr_2O_3 is dominated by direct exchange. The Néel temperature is calculated using the pair-cluster approximation for localized quantum spins of magnitude $3/2$. Very good agreement with experiment is found for all properties including the equilibrium volume, spectral density, local magnetic moment, band gap, and the Néel temperature for the values of U and J that are close to those obtained within the constrained occupation method. The band gap is of the Mott-Hubbard type.

Corundum-type Cr_2O_3 is one of the antiferromagnetic transition-metal oxides which present a significant challenge for electronic band theory due to the correlated character of the partially filled, spin-polarized $3d$ shell. It also has numerous applications in electronic devices, fuel cell electrodes, gas sensors, heterogeneous catalysis, and thermal barrier coatings. Surface properties of Cr_2O_3 are of particular interest. The nominally polar, but compensated (0001) surface exhibits structural phase transitions which are poorly understood,^{1,2} as well as an uncompensated surface moment³ which may be useful in spintronic applications. It is therefore very desirable to establish whether electronic correlations can be reliably included in first-principles calculations in a way that would accurately predict structural, electronic, and magnetic properties.

As expected for a transition-metal oxide, conventional density-functional theory (DFT) studies of bulk Cr_2O_3 ^{4,5,6} have shown that local spin density approximation (LSDA) or the generalized-gradient approximation (GGA) for the exchange-correlation potential are unable to reproduce the electronic and magnetic properties of bulk Cr_2O_3 . Rohrbach *et al.*⁷ performed a GGA+U calculation for Cr_2O_3 using the simplified (spherically averaged) $U - J$ correction⁸ and obtained more reasonable results for the band structure. However, this approach is inaccurate for structural and magnetic properties. First, as is typical for transition-metal compounds, both GGA and the LSDA+U corrections reduce the LSDA overbinding problem in Cr_2O_3 and increase the equilibrium volume which becomes close to the experimental value. However, the use of *both* GGA and Hubbard U in the GGA+U method⁷ results in an overcorrection, so that the equilibrium volume becomes 7% too large. Also, the magnetic energies found by Rohrbach *et al.* within this method are incompatible with the experimental Néel temperature of about 308 K; they are too small roughly by a factor of 5. Mosey *et al.*⁹ calculated the U and J parameters using the unrestricted Hartree-Fock method and found $U - J = 7.7$ eV, which is quite obviously too

large for Cr, as is typical for Hartree-Fock-like methods. They also studied the structural and electronic properties of Cr_2O_3 using the spherically averaged LSDA+U implementation⁸ and found that the structural properties and the band gap come out best at $U - J = 4$ eV. For this value of $U - J$ the magnetic moment is somewhat reduced from the “ideal” (ionic) value of $3 \mu_B$ due to hybridization with oxygen, which is also in agreement with experimental data.¹⁰

In this paper we analyze the properties of Cr_2O_3 in more detail with a particular emphasis on its magnetism. We found that the LSDA+U method can provide very good agreement with experiment for structural, spectral, and magnetic properties with the same values of U and J which are close to those found from the constrained occupation method within DFT.

The first-principles calculations were carried out using the projected augmented wave (PAW) method^{11,12} implemented within the Vienna *ab initio* simulation package (VASP).^{13,14} The $2s$ states on O were treated as valence states. We used the rhombohedral primitive cell for the corundum structure in all calculations except those involving complicated magnetic configurations (see below). The Monkhorst-Pack scheme¹⁵ based on the $4 \times 4 \times 4$ k -point grid was employed for the Brillouin zone integrals, which were calculated using the tetrahedron method with Blöchl corrections. The plane-wave energy cutoff was 520 eV. These parameters ensured the total energy convergence to 2 meV/atom. Densities of states (DOS) were calculated using the $8 \times 8 \times 8$ k -point grid.

We employ the LSDA+U method in its full spherically symmetric form.¹⁶ This extension is important for Cr_2O_3 where correct representation of crystal field and exchange splittings within the partially filled $3d$ shell is critical. Surface energetics are even more sensitive to the correct treatment of these unfilled shells; in fact, we found that the errors introduced by the spherically averaged LSDA+U ansatz are intolerable for the $\text{Cr}_2\text{O}_3(0001)$ surface.¹⁷ The double-counting term is taken in the fully localized limit.^{16,18}

Reasonable values of U and J can usually be obtained within DFT using the constrained occupation method.¹⁹ These values are better suited for use in LSDA+ U calculations compared to the Hartree-Fock values, because they include the screening of the $3d$ shell by the remaining electrons. We calculated U and J in this way using the full-potential linear augmented plane-wave (FLAPW) method implemented in the FLEUR package.²⁰ In these calculations the GGA approximation was used. We took the rhombohedral primitive cell of Cr_2O_3 containing four Cr atoms and set all the structural parameters to their experimental values.²¹ The $3d$ electrons on one or two (most distant) Cr atoms were formally treated as open core shells, i.e. an integer occupation of these orbitals (for each spin projection) was enforced, and their hybridization with all other electrons was turned off. The U and J parameters are then found by comparing the LSDA total energies for different charge and spin occupations of the $3d$ orbital(s) with their Hartree-Fock expressions (the latter are equal to the “double-counting” terms in LSDA+ U).

The constrained occupation method is somewhat ambiguous because the U parameter depends on the charge state of the ion²². (On the contrary, the J parameter is usually very well defined; we found this to be the case for Cr_2O_3 as well.) Although the formal charge state of the chromium ion is Cr^{3+} , we find U and J with respect to the $3d^4$ state. The reason is that the screening properties of the valence electrons depend primarily on the charge density distribution in the crystal, which is typically very close to the superposition of atomic charge densities. Indeed, the formal occupancy of the Cr $3d$ orbital within the 2.5 a.u. muffin tin sphere is about 4.2 in FLAPW. Specifically, the exchange parameter $J = 0.58$ eV was found by treating $3d$ electrons on one Cr atom as core and considering the energy difference between the $3d_{\uparrow}^2 3d_{\downarrow}^2$, $3d_{\uparrow}^3 3d_{\downarrow}^1$ and $3d_{\uparrow}^4 3d_{\downarrow}^0$ configurations. The Hubbard parameter $U = 3.3$ eV was found by treating the $3d$ shells on the two most distant Cr atoms as open cores and considering the energy difference between the $3d_{\uparrow}^4 3d_{\downarrow}^4$ and $3d_{\uparrow}^5 3d_{\downarrow}^3$ configurations, where 1 and 2 refer to the two different sites (the contribution of J to the energy differences was subtracted). Since the total number of electrons in the cell is the same for both configurations, there is no need to include the Fermi level correction.

In the following calculations we fixed J at its calculated value of 0.58 eV and varied U . The electronic structure is calculated in the ground antiferromagnetic state with relaxed structural parameters (commonly denoted as $+ - + -$ in accordance with the ordering of Cr spins along the z axis of the rhombohedral cell). The dependence of the equilibrium volume, magnetic moment, and band gap on U is shown in Fig. 1. We see that the volume and the band gap agree quite well with experimental data at $U = 4$ eV. Other structural parameters also agree with experiment. The calculated angle between the rhombohedral unit vectors is 55.11° compared to the measured²¹ angle of 55.13° . The shortest distance between Cr atoms

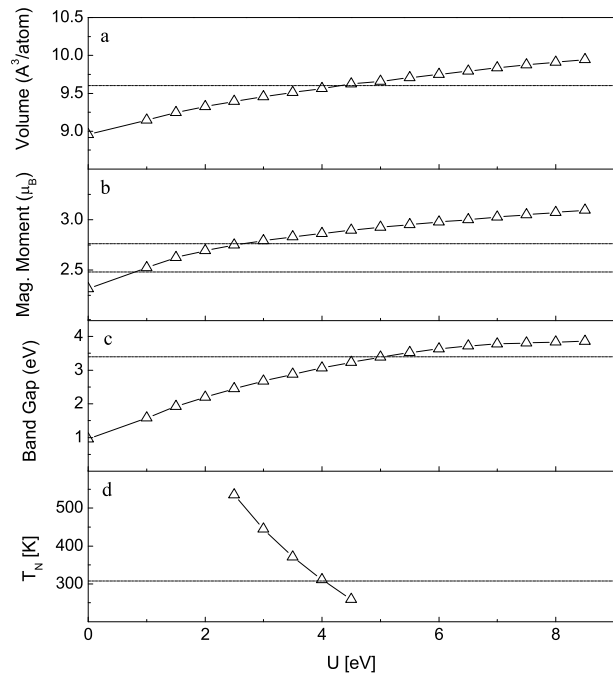


FIG. 1: Atomic volume (a), magnetic moment (b), band gap (c) and Néel temperature (d) as functions of the Coulomb U parameter for the antiferromagnetic $+ - + -$ state. The value of J is fixed at 0.58 eV. The horizontal lines denote experimental values; those in panel (b) are from both Refs. 23,24.

along the $[111]$ axis is 2.646 \AA vs the measured 2.650 \AA .

The magnetic moment at $U = 4.0$ eV is $2.86 \mu_B$, i.e. it is somewhat reduced compared to the “ideal” ionic value of $3 \mu_B$ corresponding to a fully localized spin $3/2$. Experimentally, the most recent neutron polarimetry measurement gives the sublattice magnetization of $2.48 \mu_B$ ²³, which is notable lower compared to an older estimate of $2.76 \mu_B$.²⁴ The magnetic moment is smaller than $3 \mu_B$ due to two effects: (1) hybridization with oxygen, which is included in our calculation, and (2) the quantum “zero-point spin deviation,” which is absent in DFT. The zero-point deviation in Cr_2O_3 was estimated²⁵ to be about 8%, which amounts to $0.24 \mu_B$. Thus, keeping in mind the uncertainties related to the *definition*, measurement, and calculation of the magnetic moment, its calculated value at $U \approx 4.0$ eV is completely reasonable. Of course, the poorly defined reduction from $3 \mu_B$ can not be used as an indicator of the quality of agreement with experiment. We also note that the local magnetic moment depends very weakly on the magnetic configuration of Cr_2O_3 . In the ferromagnetic state the local moment within the muffin-tin sphere is $2.94 \mu_B$, while the *magnetization* is exactly equal to $3 \mu_B$ per Cr site, as expected. The orbital moment in the calculation with spin-orbit coupling is small (about $0.04 \mu_B$) and antiparallel to the spin moment, in agreement with the experimental²⁶ g -factor of 1.97 and with the general rule for atomic shells that are less than half filled.

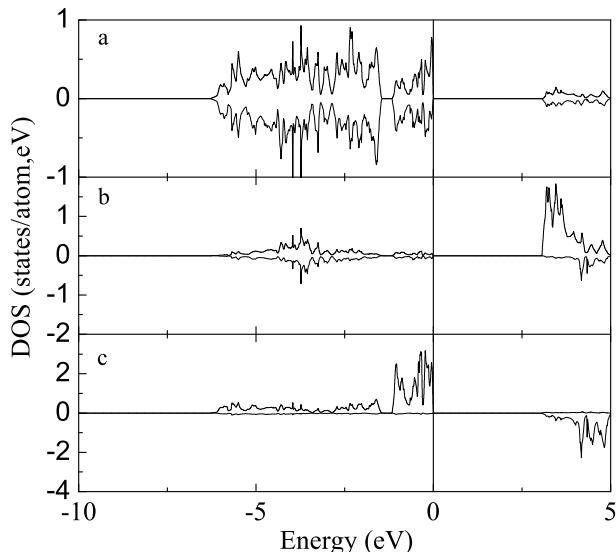


FIG. 2: Orbital projected DOS for the antiferromagnetic $+ - + -$ ground state of bulk Cr_2O_3 , calculated within the LSDA+U with $U = 4.0$ eV, $J = 0.58$ eV. (a) O-2p, (b) Cr- e_g and (c) Cr- t_{2g} . Majority and minority-spin DOS are plotted with different signs.

The band gap of 3.07 eV is somewhat smaller than the experimental value of 3.4 eV, but greater than that found in Ref. 7 using GGA+U with $U - J = 4$ eV. Underestimation of the addition energy is a common feature of the LSDA+U method, which is well known, for example, for Gd and other $4f$ elements. Further, the density of states shown in Fig. 2 is in excellent agreement with X-ray photoemission data^{27,28}. Namely, the sharp and narrow peak at low binding energies separated by a (pseudo)gap from the rest of the valence band is very well reproduced. Fig. 2 also shows the partial DOS decomposition into O and Cr contributions from t_{2g} and e_g states. (The t_{2g} and e_g subbands are well defined because the ligand field of the Cr site is approximately octahedral.) As seen from Fig. 2, the peak at low binding energies corresponds to the filled Cr t_{2g} spin subband with some admixture of oxygen p orbitals. At least some of this admixture is fictitious, because the Cr d orbitals extend into oxygen's projection spheres. (The same ambiguity is involved in the definition of the Cr magnetic moment.) Since non-magnetic Cr_2O_3 is metallic with the Fermi level lying inside the t_{2g} subband which is separated by a gap from the oxygen p band, the insulating gap forms by the Mott-Hubbard mechanism.

Thus, the available structural and spectral properties of Cr_2O_3 are well reproduced by the spherically symmetric LSDA+U method with $U \approx 4.0$ eV and $J = 0.58$ eV. This value of U is somewhat larger than that given by the constrained occupation method, but the latter was found using FLAPW calculations with a different muffin-tin radius.

We now focus on the magnetic energetics which

TABLE I: The exchange parameters J_n fitted using the total energies of 12 magnetic configurations calculated for different values of U with J fixed at 0.58 eV. Each pair of sites contributes $J_{ij}\mathbf{e}_i\mathbf{e}_j$ to the total energy, where \mathbf{e}_i is the unit vector parallel to the direction of the local moment at site i . The last column Δ shows the mean-square misfit in the fitting of the total energy. J_n and Δ are given in meV.

U	J_1	J_2	J_3	J_4	J_5	Δ
2.5	30.9	21.9	-0.60	-1.83	4.92	0.91
3.0	23.9	17.3	-1.26	-2.36	3.72	0.62
3.5	18.6	13.8	-1.74	-2.72	2.84	0.43
4.0	14.6	11.1	-2.11	-2.96	2.16	0.30
4.5	11.1	9.04	-2.41	-3.11	1.64	0.20

provides another stringent test of the validity of the LSDA+U method for Cr_2O_3 . We calculated the total energies of 12 different magnetic configurations including the ferromagnetic state, three simple antiferromagnetic orderings ($+ - + -$, $+ + - -$, and $+ - - +$), and eight additional, arbitrarily chosen spin configurations in the hexagonal unit cell of the corundum structure which includes six formula units. The ground antiferromagnetic state has $+ - + -$ ordering in agreement with experiment; its relaxed structure was fixed for other magnetic orderings. The calculated total energies are well fitted by the conventional Heisenberg Hamiltonian with exchange interaction in five coordination spheres. The exchange parameters fitted by the least squares method for different values of U are listed in Table I. The first, second and fifth nearest-neighbor interactions are antiferromagnetic, whereas the third and fourth ones are ferromagnetic. All exchange parameters except the third one reinforce the ground state. Also, we see that the first and second exchange parameters are significantly larger than those for more distant neighbors; this behavior is natural for an insulator. In Cr_2O_3 the parameter J_1 corresponds to the short bond along the z axis, and J_2 to the nearest neighbor bond within the buckled Cr layer. Each Cr atom has one J_1 neighbor and three J_2 neighbors. As the value of U is increased, all antiferromagnetic exchange parameters systematically decrease, while the ferromagnetic parameters systematically increase.

Let us compare our results with those derived from the spin wave dispersion measured by inelastic neutron scattering.²⁵ The exchange parameters fitted to those dispersion curves are also dominated by antiferromagnetic J_1 and J_2 . However, more distant neighbors in that fitting²⁵ are much less important. For example, $J_5/J_1 \approx 1/40$ in Ref. 25 *vs* $1/7$ found here. Also, there is a notable disagreement in the J_2/J_1 ratio: Ref. 25 found $J_2/J_1 \approx 0.45$ versus 0.76 for $U = 4$ eV in Table I. We have verified that the anisotropy J_2/J_1 is almost unchanged if only the lowest-lying spin configurations are included in the fitting.

We also considered the possibility that the exchange

parameters may be affected by lattice distortion below the Néel temperature due to magnetostructural coupling. In order to study this possibility, we need to know how the exchange parameters depend on the structural parameters, and how the latter change between room temperature and liquid nitrogen temperature where the spin wave spectrum was measured. We found that the values of J_1 and J_2 are very sensitive to the lattice parameters; a 1% increase or decrease in the first or second neighbor bond length leads to a 25-50% decrease or increase of the corresponding exchange parameter (this was roughly established by varying the Bravais lattice parameters of the rhombohedral cell and fitting the four simple magnetic orderings to the Heisenberg model). Thus, the J_2/J_1 ratio is very sensitive to the c/a ratio (or any lattice distortion that changes the ratio of the first and second bond lengths R_2/R_1).

To our knowledge, no experimental data are available on the thermal contraction of Cr_2O_3 below room temperature. In order to assess the degree of magnetostructural coupling, we have fully relaxed the structure for all the 12 magnetic configurations that were included in the fitting of exchange parameters. The magnetostructural coupling is, in general, quite appreciable; the R_2/R_1 ratio varies between the minimum of 1.072 in the $+-+$ configuration (where the nearest-neighbor pairs are all parallel, and next-nearest antiparallel) and the maximum of 1.103 in the $++--$ configuration (where the situation is reversed). The overall trend, as expected in general for antiferromagnetic coupling, is for each of these bonds to shorten when the corresponding spins are antiparallel and lengthen when they are parallel. Although this effect seems to be rather large, the actual $+-+$ state has *both* first and second-neighbor pairs antiparallel, so that both should lengthen somewhat in the paramagnetic state. Among our 12 configurations, 5 have the same ratio $N_P^{(i)}/N_{AP}^{(i)}$ of the number of parallel and antiparallel pairs in the i -th coordination sphere for $i = 1$ and $i = 2$, i.e. these 5 configurations approximately represent the change of structure as a function of the antiferromagnetic order parameter. The R_2/R_1 ratio for these 5 structures varies between 1.088 in the $+-+$ state and 1.084 in the ferromagnetic state. The 3 intermediate states, all of which have twice as many parallel pairs than antiparallel ones, all have $R_2/R_1 = 1.087$. The bond lengths themselves change by about 0.7% between the $+-+$ state and these three intermediate states. This variation is obviously too small to explain the disagreement with experiment in the J_2/J_1 ratio.

Thus, in spite of the overall agreement with experiment for most properties, a discrepancy in the J_2/J_1 ratio remains. It is possible that our Heisenberg model fitting is not fully applicable to small deviations from the ground state, for which the linear response technique should be a better fit. Further, spin waves are more sensitive to distant couplings compared to the energy fits or thermodynamic properties, which makes the fits from spin wave data and from the overall energetics statistically inequival-

alent. Finally, many-body effects beyond LSDA+U may play a role in renormalizing the exchange parameters. We also note that impurities and thermal spin disorder should be more effective in destroying distant couplings compared to nearest-neighbor ones; this may explain the larger role of couplings beyond J_2 in our fitting compared to experimental spin wave results.

The mechanisms of exchange interaction in Cr_2O_3 are not well understood. Complicated crystal structure with the presence of many electronic orbitals of different symmetry and many Cr-O-Cr links at different angles greatly complicates the empirical analysis. Both superexchange and direct exchange interactions have been invoked to explain the magnetic structure of Cr_2O_3 .^{29,30,31,32} Direct exchange interaction may be interpreted in terms of hopping of electrons from one Cr ion to another across the insulating gap; the energy denominator involved in this process is the Mott-Hubbard splitting. The hopping can only be effective between the orbitals that are able to hybridize. From the DOS decomposition shown in Fig. 2 it is clear that the t_{2g} orbitals very weakly hybridize with e_g orbitals on the neighboring Cr atoms. Therefore, the contribution of e_g orbitals to direct exchange can be neglected. The t_{2g} subband is split off by crystal field and exactly half-filled, therefore direct exchange should be antiferromagnetic. The superexchange involves hopping between Cr and O ions; the energy denominator involves the gap between the oxygen p states and the unoccupied Cr states.

In order to reveal the mechanism responsible for exchange interaction in Cr_2O_3 , we use the following trick. A fictitious external potential V is coupled to the oxygen p orbitals, which adds the term $E_V = V \text{Tr} n_{mm}^\sigma$ to the total energy, where the trace is taken over orbital and spin indices, and n_{mm}^σ is the density matrix of the oxygen p states defined inside the muffin tin sphere of 1.2 a.u. This density matrix is calculated using the standard LSDA+U machinery. When V is set to a negative value, the filled oxygen p states are pushed down to lower energies, which suppresses superexchange, but not direct exchange. Weak hybridization between the filled t_{2g} states and the oxygen p states pushes them apart at $V = 0$. When the p states are pushed down by increasing V , this repulsion is reduced and the t_{2g} states also move down, thereby increasing the band gap. Since direct exchange is sensitive to the band gap, for better comparison we compensate this increased band gap by reducing U on Cr. This is done in such a way that the distance between the center of mass of the filled t_{2g} band and the conduction band minimum (CBM) remains the same as at $V = 0$.

Starting from the state with $U = 3.5$ eV, we added V of -12 eV and -24 eV and calculated the energies of four magnetic states in the rhombohedral primitive cell of Cr_2O_3 . These calculations were performed using the FLAPW method;²⁰ the results are listed in Table II. (Those for $V = 0$ are within 10% of VASP results.) The self-consistent downward shift of the p states is much smaller than $V n_{mm}$ because V is strongly screened. The

TABLE II: Energies of three simple magnetic configurations relative to the ground $+-+-$ state (in meV per formula unit) as a function of the fictitious external potential V applied to the oxygen p orbitals (in eV). Reduced values of U on Cr compensate for the increased band gap (see text for details). Δ is the distance from the oxygen band top to CBM in eV.

V	U	Δ	++++	++--	+-+-
0	3.5	4.5	130	124	66
-12	3.5	5.8	115	102	59
-12	2.5	5.6	154	128	74
-24	3.5	7.9	102	80	51
-24	2.15	7.7	145	110	71

distance Δ from the oxygen p band maximum to CBM is also listed in the table.

The results listed in Table II clearly show that the magnetic energies are insensitive to the position of the oxygen p band. The reduction of magnetic energies produced by adding negative V at constant U is due to the fact that the t_{2g} band gap increases due to dehybridization from oxygen. Once U is decreased to bring the band gap to its original value, the magnetic energies are essentially unchanged compared to their values at $V = 0$; in fact, they even increase somewhat. On the other hand, we've seen above that the magnetic energies are very sensitive to the value of U which is responsible for the band gap. This behavior leads us to a striking conclusion that, contrary to the common belief, superexchange plays no role in magnetism of Cr_2O_3 . Antiferromagnetism is due exclusively to direct exchange, which, as mentioned above, is antiferromagnetic because the magnetically active t_{2g} subband is half-filled. It is likely that superexchange in Cr_2O_3 is highly ineffective because the Cr-O-Cr angles are close to 90° , while the overlap between O states and Cr t_{2g} states is small. On the other hand, the overlaps between t_{2g} states on neighboring Cr atoms are quite large; the t_{2g} bandwidth in the ferromagnetic state at $V = -24$ eV is approximately 1.5 eV.

We now calculate the Néel temperature T_N . We saw above that the local moments on Cr atoms are well localized, and the energies of spin configurations are well represented by the Heisenberg spin Hamiltonian. We therefore adopt the quantum Heisenberg model for localized spins of magnitude $3/2$ with the exchange parameters listed in Table I. Since each spin is strongly coupled only to four neighbors (one with J_1 and three with J_2), the mean-field approximation can not be reliably used. However, the antiferromagnetic interaction is not frustrated. The important spin correlations should be generated by the dominant exchange interaction with four nearest neighbors. The network of bonds corresponding to J_1 and J_2 is very weakly connected; the shortest closed path on this network is 6 bonds long. Therefore, it is sufficient to capture the pairwise spin correlations. In this situation, the pair cluster approximation appears to be

an obvious choice. This approach is a special case of the cluster variation method when the set of clusters includes only pairs of sites. Here we follow the formulation of Ref. 33 which can be directly applied to our case. The details of this technique are described in the Appendix.

The calculated T_N is shown in Fig. 1 as a function of U . We see that the best agreement with experiment for T_N is obtained at the same value of $U \approx 4$ eV as for the structural and spectral properties explored above. This overall agreement is a strong indication that the essential details of the electronic structure of Cr_2O_3 are very well captured by the LSDA+U approximation. Physically, this success of LSDA+U is explained by the presence of fully filled and empty subbands which are strongly split by crystal and exchange fields; LSDA+U usually reproduces such closed atomic-like subshells very well.

In conclusion, we found that the spherically symmetric LSDA+U method provides a very good description of structural, spectral, and magnetic properties of chromia with $J = 0.58$ eV found from the constrained occupation method and $U \approx 4$ eV, which is also close to the calculated value. We found that the magnetic energies are well represented by a Heisenberg model with strong exchange interaction with nearest neighbors both in the plane and along the z axis and much weaker interaction with more distant neighbors. The artificial downward shift of the filled oxygen p states has almost no effect on the magnetic energies, which proves that direct exchange is the dominant mechanism of magnetic interaction.

This work was supported by NRC/NRI supplement to NSF-MRSEC and by the Nebraska Research Initiative. K. B. is a Cottrell Scholar of Research Corporation.

APPENDIX

Here we describe the application of the pair cluster approximation to Cr_2O_3 following a similar formalism of Ref. 33. The energy of a quantum Heisenberg magnet (per unit cell) can be written as

$$E = -\frac{1}{2} \sum_{i,j} m_i n_{ij} J_{ij} \langle \hat{\mathbf{S}}_i \cdot \hat{\mathbf{S}}_j \rangle - \sum_i m_i B_i \langle \hat{S}_i^z \rangle, \quad (\text{A.1})$$

where the summations are over the inequivalent sites in the unit cell, $\hat{\mathbf{S}}_i$ are quantum spin operators, m_i is the number of sites of type i in the unit cell, n_{ij} the number of neighbors of site i that are of type j , and B_i the external magnetic field applied to site type i . All the thermodynamic properties can be obtained from the free energy which may be calculated by integrating the Gibbs-Helmholtz relation:

$$F = \frac{1}{\beta} \int_0^\beta E(\beta') d\beta', \quad (\text{A.2})$$

To proceed we need to find the expectation values appearing in Eq. (A.1). In the pair-cluster approximation

they are calculated by introducing one- and two-site clusters with the following cluster Hamiltonians:

$$\begin{aligned}\hat{H}_1^i &= -h_i \hat{S}_i^z \\ \hat{H}_2^{ij} &= -J_{ij} \hat{\mathbf{S}}_i \cdot \hat{\mathbf{S}}_j - h_i^{(j)} \hat{S}_i^z - h_j^{(i)} \hat{S}_j^z,\end{aligned}\quad (\text{A.3})$$

where $h_i = B_i + \phi_i$ is the one-site ‘‘cluster field,’’ $h_i^{(j)} = h_i - \phi_i^{(j)}$ is the cluster field at site i for the pair cluster (i, j) . The one-site and two-site cluster fields are related through $\phi_i = \sum_j n_{ij} \phi_i^{(j)}$. The quantities $\phi_i^{(j)}$ are treated as variational parameters and found by minimizing the free energy, i.e. requesting that $\partial F / \partial \phi_i^{(j)} = 0$. It can be shown that this variational condition ensures that the expectation value $\langle \hat{S}_i^z \rangle$ is the same in all one-site and all two-site clusters containing site i . The expectation values $\langle \hat{\mathbf{S}}_i \cdot \hat{\mathbf{S}}_j \rangle$ are calculated from the pair cluster (i, j) . Performing the integration in (A.2), we find

$$F = -\frac{1}{2\beta} \sum_{ij} m_i n_{ij} \ln Z_2^{ij} + \frac{1}{\beta} \sum_i m_i (n_i - 1) \ln Z_1^i, \quad (\text{A.4})$$

where $n_i = \sum_j n_{ij}$ is the total number of neighbors of site i , while $Z_1^i = \text{Tr} \exp(-\beta H_1^i)$ and $Z_2^{ij} = \text{Tr} \exp(-\beta H_2^{ij})$ are the one-site and two-site cluster partition sums. Evaluation of Z_1^i is trivial; to find Z_2^{ij} one first needs to diagonalize H_2^{ij} .

Our goal here is to find the transition temperature; therefore we may assume that all $h_i^{(j)}$ are small. The free energy is developed in these parameters, and then the parameters $\phi_i^{(j)}$ are found by requiring that the variation of the free energy F vanishes. (The resulting equations are too cumbersome to be included here.)

For Cr_2O_3 we assume the actual magnetic ordering $+ - + -$. All Cr sites are related by magnetic symmetry, which reduces the number of independent variational parameters. The transition temperature is found by setting $S = 3/2$ and searching for the pole of the magnetic susceptibility which is found from the one-site cluster:

$$\chi_{ij} = \frac{\partial \langle S_i^z \rangle}{\partial B_j} = \frac{S(S+1)}{3} \beta \frac{\partial h_i}{\partial B_j}. \quad (\text{A.5})$$

The resulting equation for the transition temperature has two solutions. The greater solution is T_N , while the lower one is the fictitious ‘‘anti-Néel point’’ below which $\langle \hat{S}_i^z \rangle = 0$. The existence of an anti-Néel point for antiferromagnets is a well-known shortcoming of the pair-cluster approximation,^{33,34} which fails at low temperatures. However, in our case the anti-Néel point is much smaller than T_N which indicates that the pair cluster approximation has a wide range of validity. Therefore, this method is expected to provide a very good approximation for T_N .

* Present address: Department of Physics, Center for Optoelectronics Materials and Devices, Zhejiang Sci-Tech University, Xiasha College Park, Hangzhou 310018, China.

¹ M. Bender, D. Ehrlich, I. N. Yakovkin, F. Rohr, M. Bäumer, H. Kuhlenbeck, H.-J. Freund, and V. Staemmler, *J. Phys.: Condens. Matter* **7**, 5289 (1995).

² Th. Gloege, H. L. Meyerheim, W. Moritz, and D. Wolf, *Surf. Sci.* **441**, L917 (1999).

³ S. Sahoo and Ch. Binek, *Phil. Mag. Lett.* **87**, 259 (2007).

⁴ M. Catti, G. Sandrone, G. Valerio, and R. Dovesi, *J. Phys. Chem. Solids* **57**, 1735 (1996).

⁵ A. Y. Dobin, W. Duan, and R. M. Wentzcovitch, *Phys. Rev. B* **62**, 11997 (2000).

⁶ K. Wolter, D. Scarano, J. Fritsch, H. Kuhlenbeck, A. Zecchina, and H. -J. Freund, *Chem. Phys. Lett.* **320**, 206 (2000).

⁷ A. Rohrbach, J. Hafner, and G. Kresse, *Phys. Rev. B* **70**, 125426 (2004).

⁸ S. L. Dudarev, G. A. Botton, S. Y. Savrasov, C. J. Humphreys, and A. P. Sutton, *Phys. Rev. B* **57**, 1505 (1998).

⁹ N. J. Mosey and E. A. Carter, *Phys. Rev. B* **76**, 155123 (2007).

¹⁰ Refs. 7 and 9 concluded that there is a large disagreement with experiment in the magnetic moment, but they used an incorrect experimental value of $3.8 \mu_B$.

¹¹ P. E. Blöchl, *Phys. Rev. B* **50**, 17953 (1994).

¹² G. Kresse, and D. Joubert, *Phys. Rev. B* **59**, 1758 (1999).

¹³ G. Kresse, and J. Hafner, *Phys. Rev. B* **48**, 13115 (1993).

¹⁴ G. Kresse, and J. Furthmüller, *Phys. Rev. B* **54**, 11169 (1996).

¹⁵ H. Monkhorst, and J. D. Pack, *Phys. Rev. B* **13**, 5188 (1976).

¹⁶ A. I. Liechtenstein, V. I. Anisimov, and J. Zaanen, *Phys. Rev. B* **52**, R5467 (1995).

¹⁷ Siqi Shi and K. D. Belashchenko (unpublished).

¹⁸ A. G. Petukhov, I. I. Mazin, L. Chioncel, and A. I. Liechtenstein, *Phys. Rev. B* **67**, 153106 (2003).

¹⁹ V. I. Anisimov and O. Gunnarsson, *Phys. Rev. B* **43**, 7570 (1991).

²⁰ S. Blügel and G. Bihlmayer, in *Computational Nanoscience: Do It Yourself!*, edited by J. Groten-dorst, S. Blügel, and D. Marx, John von Neumann Institute for Computing, Jülich, NIC Series, Vol. **31**, p. 85 (2006). See www.flapw.de.

²¹ L. W. Finger and R. M. Hazen, *J. Appl. Phys.* **51**, 5362 (1980).

²² I. V. Solovyev, and P. H. Dederichs, *Phys. Rev. B* **49**, 6736 (1994).

²³ P. J. Brown, J. B. Forsyth, E. Lelièvre-Berna, and F. Tasset, *J. Phys.: Condens. Matter* **14**, 1957 (2002).

²⁴ L. M. Corliss, J. M. Hastings, R. Nathans, and G. Shirane, *J. Appl. Phys.* **36**, 1099 (1965).

²⁵ E. J. Samuelsen, M. T. Hutchings, and G. Shirane, *Physica* **48**, 13 (1970).

²⁶ S. Foner, *Phys. Rev.* **130**, 183 (1963).

²⁷ R. Zimmermann, P. Steiner, and S. Hüfner, *J. Electron Spectrosc. Relat. Phenom.* **78**, 49 (1996).

- ²⁸ T. Uozumi, K. Okada, A. Kotani, R. Zimmermann, P. Steiner, S. Hüfner, Y. Tezuka, and S. Shin, *J. Electron Spectrosc. Relat. Phenom.* **83**, 9 (1997).
- ²⁹ Y. Y. Li, *Phys. Rev.* **102**, 1015 (1956).
- ³⁰ S. Iida, *J. Phys. Soc. Japan* **11**, 1300 (1956).
- ³¹ J. B. Goodenough, *Phys. Rev.* **117**, 1442 (1960).
- ³² W. P. Osmond, *Proc. Phys. Soc.* **79**, 394 (1962).
- ³³ V. G. Vaks and N. E. Zein, *Sov. Phys. JETP* **40**, 537, (1975).
- ³⁴ P. W. Kasteleijn and J. van Kranendonk, *Physica* **22**, 317, 367, (1956).